Low-temperature magnetic structure and electron paramagnetic resonance properties of the quasi-one-dimensional $S = \frac{1}{2}$ Heisenberg helimagnet $CuCl_2 \cdot 2NC_5H_5$

A. N. Ponomaryov,[1] L. Zviagina,[1] J. Wosnitza,[1,2] M. Thede,[3] E. Ressouche,[4,5] K. Yu. Povarov,[3] A. Zheludev,[3] C. P. Landee,[6] and S. A. Zvyagin[1]

[1]*Dresden High Magnetic Field Laboratory (HLD-EMFL), Helmholtz-Zentrum Dresden-Rossendorf, D-01328 Dresden, Germany*

[2]*Institut für Festkörperphysik, TU Dresden, D-01062 Dresden,Germany*

[3]*Neutron Scattering and Magnetism, Laboratory for Solid State Physics, ETH Zürich, 8093 Zürich, Switzerland*

[4]*Université Grenoble Alpes, 38042 Grenoble, France*

[5]*MEM-MDN, INAC, 38054 Grenoble, France*

[6]*Department of Physics and Carlson School of Chemistry, Clark University, Worcester, Massachusetts 01060, USA*

(Received 9 February 2017; published 10 May 2017)

We present results of electron paramagnetic resonance (EPR) and neutron-diffraction studies of $CuCl_2 \cdot 2NC_5H_5$, which is regarded as one of the best known uniform spin-1/2 Heisenberg antiferromagnet chain systems. We reveal that at $T_N = 1.12$ K, $CuCl_2 \cdot 2NC_5H_5$ undergoes the transition into the magnetically ordered spiral state with $Q = (0.5, 0.4, 0.5)$ r.l.u. It was shown that the zigzag interchain interactions result in a noticeable geometrical frustration, also affecting the ordered moment per Cu^{2+} and EPR properties, including the angular dependence of the linewidth. The temperature dependencies of the EPR parameters are discussed.

DOI: 10.1103/PhysRevB.95.195125

I. INTRODUCTION

Quantum fluctuations can be significantly enhanced in low-dimensional spin magnets, making these systems an ideal ground for testing various theoretical concepts of quantum magnetism [1]. An isotropic spin-1/2 Heisenberg antiferromagnetic (AF) chain with uniform nearest-neighbor exchange coupling represents one of such paradigm models. In zero field, its ground state is a spin singlet, and the spin dynamics is determined by a gapless two-particle continuum of spin-1/2 excitations, commonly referred to as spinons. The spinon excitation spectrum can be calculated using the Bethe ansatz [2]. Since the spin-1/2 chain is critical, even a small perturbation can considerably change fundamental properties of the system, including its spin dynamics. For instance, the presence of alternating (staggered) Dzyaloshinskii-Moriya (DM) interaction may result in a field-induced energy gap $\Delta \sim H^{2/3}$ (H is the applied magnetic field) [3,4], while the excitation spectrum is formed by sine-Gordon solitons and their bound states, breathers [5–10]. The presence of such excitations has been conclusively revealed by means of high-field electron spin resonance spectroscopy [11,12]. The staggered DM interaction was also found responsible for a minimum in the gap at the soliton-magnon crossover in the vicinity of the magnetization saturation field [13].

$Cu(py)_2Cl_2$ (chemical formula $CuCl_2 \cdot 2NC_5H_5$) is one of the first known and extensively studied spin-1/2 Heisenberg AF chain systems [14–27]. Despite the long history, the system still continues to attract a lot of attention. In this work, we focus on the low-energy spin dynamics and low-temperature magnetic structure of $Cu(py)_2Cl_2$ employing electron paramagnetic resonance (EPR) and neutron-diffraction techniques.

II. EXPERIMENTAL

$Cu(py)_2Cl_2$ belongs to the monoclinic $P2_1/n$ space group with parameters $a = 16.967$ Å, $b = 8.559$ Å, $c = 3.847$ Å, and $\beta = 91.98^\circ$ and two formula units ($Z = 2$) per cell [14,16,22]. Schematically, its crystal structure is shown in Fig. 1. The unit cell contains two magnetic Cu^{2+} ions (labeled as A and B; Fig. 1) with coordinates (0, 0, 0) and (1/2, 1/2, 1/2); Cu^{2+} chains are running along the c direction. The compound is characterized by the intrachain exchange interaction $J/k_B = 27.3$ K and a small interchain interaction of about 0.56 K [26]. At $T_N = 1.12$ K [18,26], the system undergoes the transition into the three-dimensional (3D) ordered state.

The $Cu(py)_2Cl_2$ single crystals were grown from solution by a slow-evaporation method at the ETH Zürich [26]. For our EPR experiments, samples of 2 mm^3 typical sizes were used. The spectra were measured employing an X-band Bruker Elexsys E500 EPR spectrometer at a frequency of 9.4 GHz. Angular dependences were measured with an accuracy better than $\pm 1^\circ$. The spectrometer was equipped with an Oxford Instruments helium-4 flow-type cryostat (model ESR900) with a lowest accessible temperature of 2 K. For accurate temperature measurements, a special EPR probe has been designed and built (Fig. 2). The probe is made out of a quartz tube with 1 mm inner and 4 mm outer diameters. A temperature sensor (LakeShore bare chip Cernox resistor, model CX-1050-BC-HT) is installed on a flat platform at the bottom of the probe. The temperature is measured by means of a four-point scheme using a LakeShore 340 bridge. The sample was mounted on the platform using Apiezon-N vacuum grease, having a direct thermal contact with the temperature sensor. No significant parasitic contribution to the EPR spectra from the probe (or cavity damping) due to the installed temperature sensor was observed.

The neutron-diffraction measurements were performed using the four-circle diffractometer D10 at the Institute Laue-Langevin (Grenoble, France). The neutron wavelength $\lambda = 2.367$ Å was provided by a pyrolytic graphite (PG) monochromator. Two different data sets were collected in two different configurations. The first one, collected with a multidetector, aimed at refining the crystal structure at low temperature. The second one, optimized for background reduction, was collected with a single detector and a PG analyzer. It was used for the

 ©2017 American Physical Society

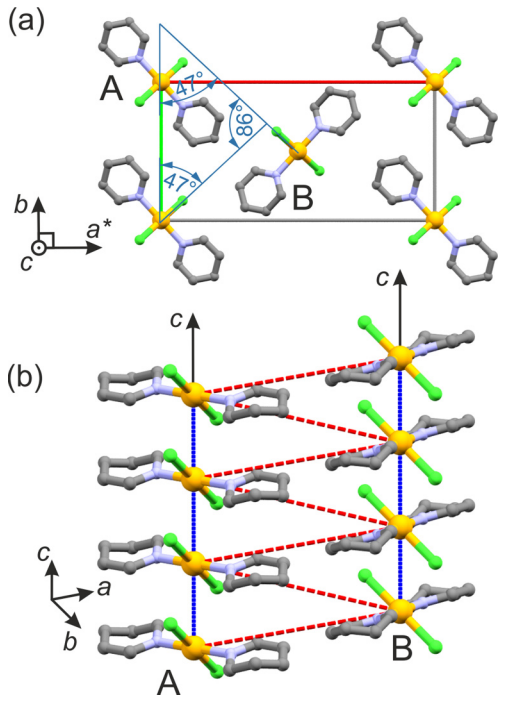

FIG. 1. Schematic view of the $Cu(py)_2Cl_2$ crystal structure. The Cu, Cl, N, and C atoms are shown in yellow, green, cyan, and gray, respectively. The hydrogen atoms are not shown for simplicity. *A* and *B* denote the two different Cu^{2+} sites (for details see the text).

magnetic-structure determination. The data collections were performed using a dilution refrigerator with a base temperature of $T = 100$ mK.

III. RESULTS AND DISCUSSIONS

The temperature dependence of the EPR spectra was measured for $H \parallel a^*$, $H \parallel b$, and $H \parallel c$, from 300 down to 2 K. A single resonance line was observed for all sample orientations. Examples of EPR spectra, obtained for $H \parallel b$ at some selected temperatures, are shown in Fig. 3. The spectra could be well described using a Lorentzian fit function; from the fit results, the linewidth (full width at half maximum, FWHM) and resonance field were extracted. For the room temperature, the g factors and linewidths, ΔH, are listed in Table I.

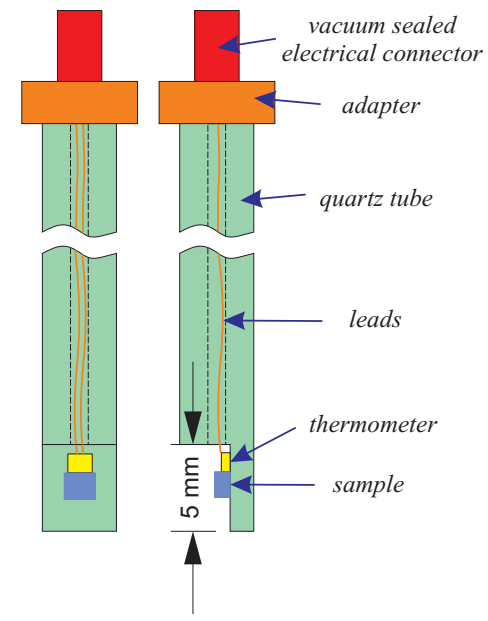

FIG. 2. Schematic front and side views of the EPR probe.

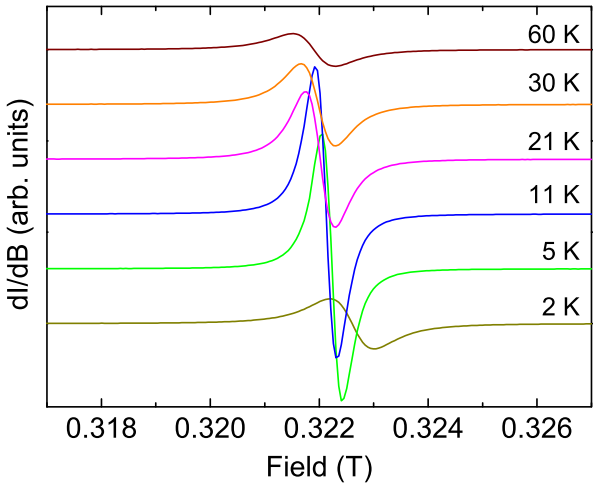

FIG. 3. Examples of EPR spectra of $Cu(py)_2Cl_2$, measured with magnetic field $H \parallel b$ at 2, 5, 11, 21, 30, and 60 K. Data are offset for clarity.

The linewidth vs temperature diagrams for $H \parallel a^*$, $H \parallel b$, and $H \parallel c$ are shown in Fig. 4.

The measurements revealed similar behavior of the EPR linewidth for all three magnetic field directions. The linewidths decrease gradually starting at room temperature, with a much steeper slope below about $T \sim J/k_B = 27.3$ K, dropping down to its minimum at $T^* \sim 7$ K. With further decreasing temperature, short-range 3D correlations become significant, leading to a low-temperature line-broadening approaching $T_N = 1.12$ K (Fig. 4). The enhancement of the 3D correlations also results in a pronounced low-temperature change of the resonance field (Fig. 5).

Now we focus on the temperature range $T^* < T < J/k_B$. At these temperatures, magnetic properties of $Cu(py)_2Cl_2$ are determined by short-range correlations within the chains. Strictly speaking, at $T = 0$ K, the EPR response of an ideal uniform spin-1/2 Heisenberg chain system with magnetically isotropic interactions should be a single absorption peak with zero linewidth. On the other hand, in the presence of magnetic anisotropy, spin-spin correlations result in a broadening of the EPR line. According to the low-temperature EPR theory [28–31] for spin-1/2 Heisenberg AF chains, the EPR linewidth is given as

$$\Delta H = \Delta H_0 + n\pi^3\lambda^2 T, \quad (1)$$

TABLE I. Room-temperature parameters of the EPR absorption lines taken for all three orientations of the magnetic field.

	$H \parallel a^*$	$H \parallel b$	$H \parallel c$
g	2.0964(3)	2.0868(3)	2.1938(3)
ΔH (mT)	1.56	1.43	1.94

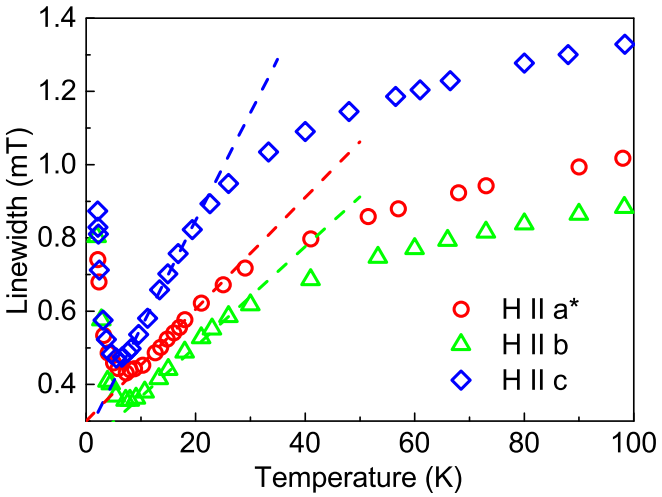

FIG. 4. Temperature dependence of the EPR linewidth. The red, green, and blue symbols correspond to data for $H \parallel a^*$, $H \parallel b$, and $H \parallel c$, respectively. The dashed lines represent linear fits using Eq. (1) in the range $T^* < T < J/k_B$ (see the text for details).

where $n = 2$ or 4 for magnetic fields applied perpendicular or parallel to the direction of the anisotropy axis, respectively, ΔH_0 is an offset, $\lambda \sim \delta/J$ for $\delta/J \ll 1$, and δ is the anisotropy parameter. Thus, from the slope of the linewidth vs temperature, we estimated δ and ΔH_0 for each direction of magnetic field. The found values are listed in Table II.

As one can see, the anisotropy parameters are in the range of several mK and can result from tiny dipole-dipole interactions present in this compound. Thus, above T_N, $Cu(py)_2Cl_2$ can be regarded as a very good realization of an isotropic spin-1/2 Heisenberg AF chain system.

The EPR angular dependence was measured at two temperatures, 300 and 10 K (sample was rotated around the c axis, while the magnetic field was applied in the a^*b plane). The corresponding angular dependences of the g factor and EPR linewidth are shown in Figs. 6 and 7, respectively.

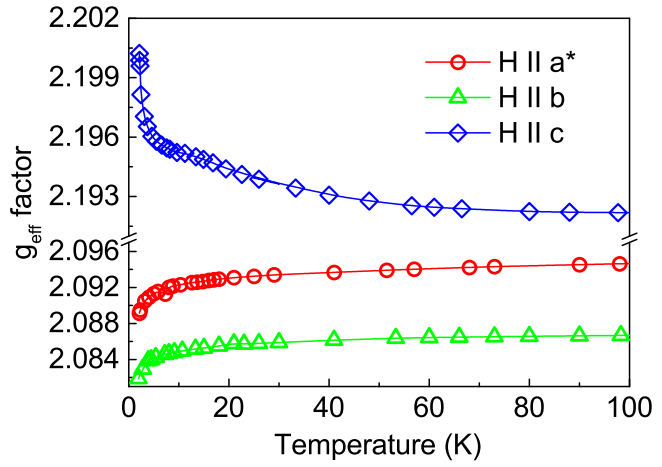

FIG. 5. Temperature dependence of the effective g factors. The red circles, green triangles, and blue diamonds represent data for $H \parallel a^*$, $H \parallel b$, and $H \parallel c$, respectively. Lines are guides to the eye.

TABLE II. A list of the parameters, extracted from the fit of EPR linewidth temperature dependence (Fig. 4) using Eq. (1).

	$H \parallel a^*$	$H \parallel b$	$H \parallel c$
ΔH_0 (mT)	0.3	0.23	0.26
δ (mK)	11	10	15

As mentioned above, $Cu(py)_2Cl_2$ contains two magnetic sites, A and B (Fig. 1), contributing to the single EPR absorption with g factor

$$g = \tfrac{1}{2}(g_A + g_B),$$

where g_A and g_B are the effective g factors for sites A and B, respectively. On the other hand, g_A and g_B can be defined as

$$g_A^2 = g_{A,\parallel}^2 \cos^2(\theta + \phi) + g_{A,\perp}^2 \sin^2(\theta + \phi) \qquad (2)$$

and

$$g_B^2 = g_{B,\parallel}^2 \cos^2(\theta + \psi) + g_{B,\perp}^2 \sin^2(\theta + \psi), \qquad (3)$$

respectively (ϕ and ψ are the effective angles, accounting for the tilting of the anisotropy axis from the a^* axis for each individual site). Assuming that both sites are identical and differ only by their orientation with respect to the unit-cell axes, one can write

$$g = \frac{1}{2}\sqrt{g_\parallel^2 \cos^2(\theta + \phi) + g_\perp^2 \sin^2(\theta + \phi)} + \frac{1}{2}\sqrt{g_\parallel^2 \cos^2(\theta + \psi) + g_\perp^2 \sin^2(\theta + \psi)}. \qquad (4)$$

Thus, fitting the angular dependence of the g factor with Eq. (4), we extract $g_\parallel$ and $g_\perp$. The fit results are shown in Fig. 6 by dashed lines and g factors are given in Table III.

Now let us turn to the angular dependencies of the linewidth. For both temperatures, there are two maxima, at $\theta \sim 50^\circ$ and $\sim 135^\circ$, which correspond to the situation when the magnetic

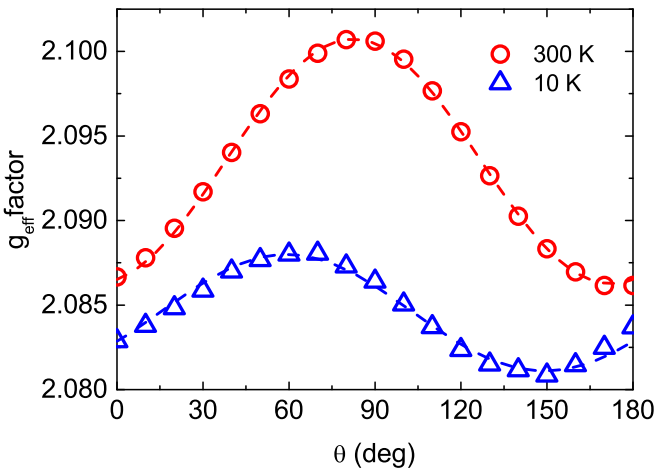

FIG. 6. Angular dependence of the g factor measured at 300 and 10 K. The sample was rotated around the c axis. The magnetic field was applied in the a^*b plane. The rotation angle θ is defined as 0° for $H \parallel b$ and, hence, is $\theta = 90^\circ$ for $H \parallel a^*$. The red circles and blue triangles represent data obtained at 300 and 10 K, respectively. The dashed lines show the fit results using Eq. (4).

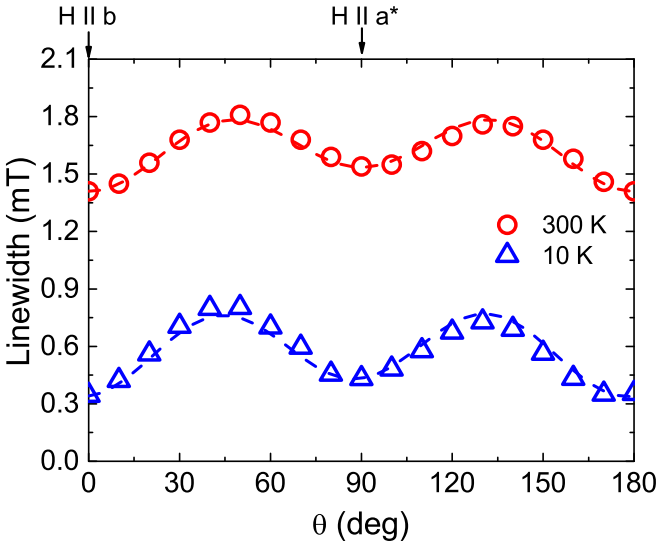

FIG. 7. Angular dependence of the EPR linewidth measured at 300 and 10 K. The sample was rotated around the c axis. The magnetic field was applied in the a^*b plane. Symbols represent experimental data and the dashed lines represent the fit results using Eq. (5).

field is applied in the basal plane formed by Cl^- ligands for one Cu^{2+} site and perpendicular to that for another one [Fig. 1(a)]. This observation is very remarkable and suggests that the frustrated zigzag interchain coupling might play an important role, resulting (as we show below) in a noncollinear magnetic structure below T_N.

We were unable to resolve two expected EPR lines from the different Cu^{2+} sites. To comment on that, let us analyze the angular dependence of the linewidth. Similar to that in Ref. [32], the EPR linewidth behavior can be described as

$$\Delta H = \Delta H_{\text{chain}} + \frac{1}{4}\frac{(g_A - g_B)^2 \mu_B H^2}{\hbar \omega_h}, \qquad (5)$$

where ω_h is the interchain hopping frequency, and $\Delta H_{\text{chain}} = \Delta H_i + \Delta H_a \sin(\theta)$ (ΔH_i and ΔH_a are the isotropic and anisotropic parts of the linewidth, respectively), g_A and g_B are defined by Eqs. (2) and (3), and H is the resonance field. The results of the fit are shown in Fig. 7 by dashed lines (the fitting revealed $\omega_h = 13.5$ and 4.1 GHz for 300 and 10 K, respectively, and other fitting parameters are given in Table III). For both temperatures, $|(g_A - g_B)|\mu_B H/\hbar\omega_h < 1$, i.e., the system is in the fast fluctuation regime [33]. This explains the absence of an EPR line splitting on this frequency scale.

TABLE III. A list of the parameters used for the fitting of the EPR linewidth angular dependence (Fig. 7) using Eq. (5).

	300 K	2 K
$g_\parallel$	2.072(1)	2.065(1)
$g_\perp$	2.115(1)	2.103(1)
H (mT)	322	322
ΔH_i (mT)	1.41	0.34
ΔH_a (mT)	0.13	0.09
ϕ, °	42.7	70.6
ψ, °	−42.7	−65.9
ω_h (GHz)	13.5	4.1

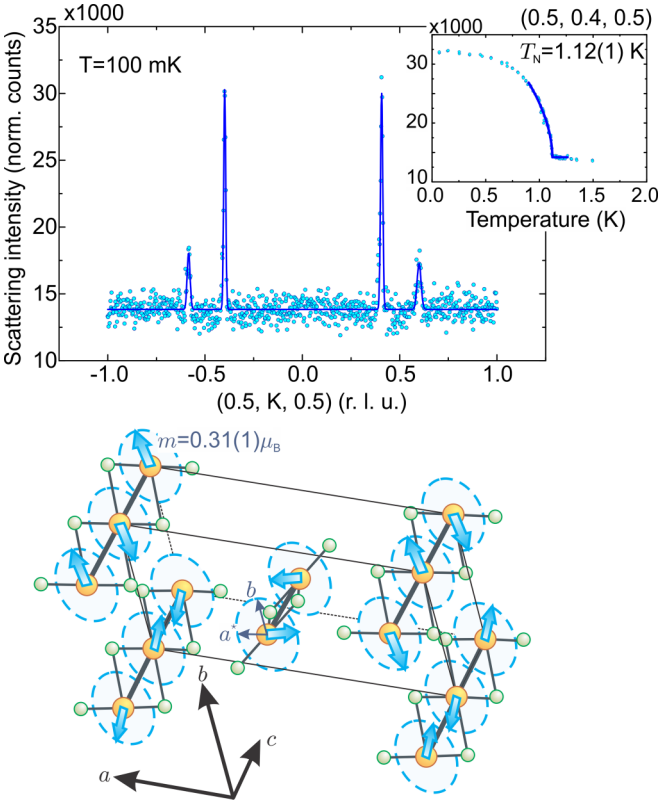

FIG. 8. Top panel: Neutron-diffraction data measured on a single crystal of $Cu(py)_2Cl_2$ with the D10 instrument. The main panel shows the low-temperature scattering intensity (normalized per neutron flux and counting time) as a function of the momentum in the (0.5, K, 0.5) direction (points) together with a fit by use of a set of Gaussian peaks (solid line). The inset shows the temperature dependence of the scattering intensity at the magnetic Bragg reflection at (0.5, 0.4, 0.5). The solid line around T_N is a guide to the eye. Bottom panel: Spin structure of $Cu(py)_2Cl_2$ ordered phase determined from the diffraction measurements.

The neutron-diffraction investigation of the magnetic structure has led to an unexpected discovery. Below $T_N = 1.12$ K, the material is 3D magnetically ordered with an incommensurate magnetic structure. The observed magnetic-structure propagation vector is $\mathbf{Q} = \pm(0.5, 0.4, 0.5)$ r.l.u.; representative magnetic Bragg peaks and the temperature dependence of one corresponding Bragg-peak intensity are shown in the top panel of Fig. 8. The structure was solved using 44 magnetic reflections at base temperature of 100 mK, with the scale factors and extinction coefficients obtained from nuclear-peak refinement. We found a helicoidal spin arrangement with the rotation plane perpendicular to the chain direction (which is the a^*b plane) [34]. This structure is shown in the bottom panel of Fig. 8. The ordered moment per Cu^{2+} site is found to be significantly reduced, $m = 0.31(1)\mu_B$. Nonetheless, we should stress that this value is still twice as large as the mean-field-theory-based expectation [26]. This discrepancy is not surprising, as the previously used mean-field theory is not appropriate in the presence of frustration, which, as the

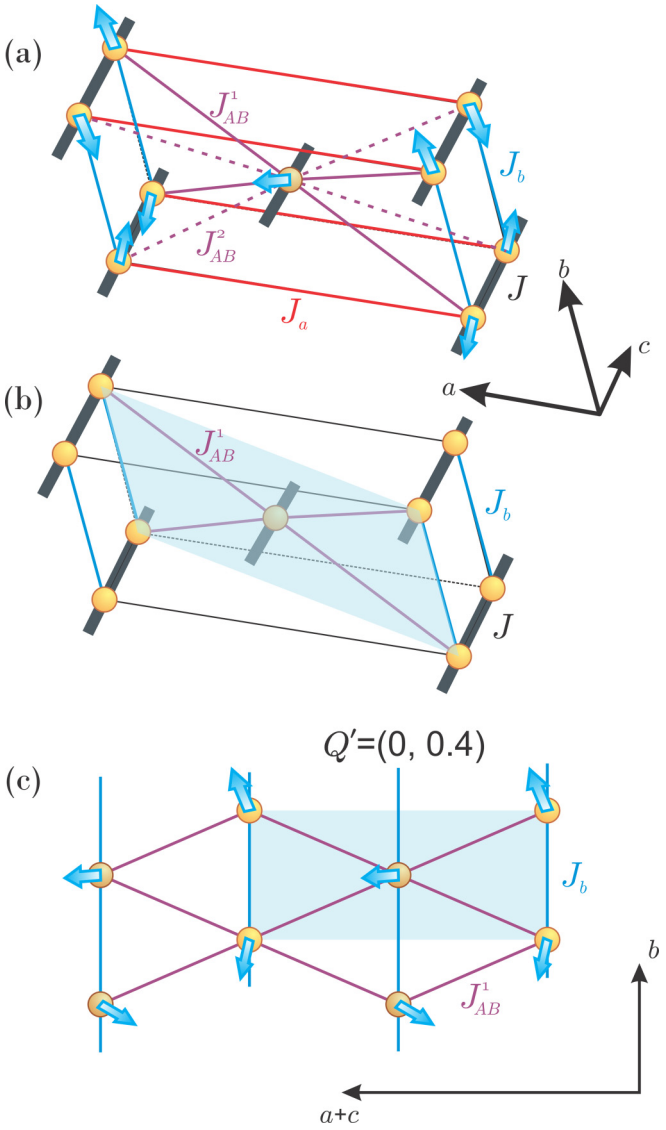

FIG. 9. (a) Most general Heisenberg exchange scheme of $Cu(py)_2Cl_2$. (b) Minimalistic model required to qualitatively capture the ground state. (c) Projection of a single triangular-lattice layer, as shown in (b).

data presented here show, is an essential ingredient in the magnetism of $Cu(py)_2Cl_2$.

The noncollinear magnetic structure in $Cu(py)_2Cl_2$ stems from the presence of the A and B positions of Cu^{2+} ions, linked by a half-period screw translation. This results in a semi-body-centered arrangement of magnetic moments within a structural unit cell, with frustrating diagonal interactions between them. The possible exchange interactions in $Cu(py)_2Cl_2$ are summarized in Fig. 9(a). The most essential is the intrachain exchange interaction J, which is sufficient to describe the thermodynamics and high-energy spectral properties [17,18,20]. In addition to the primary exchange interaction, there are two nonfrustrating interchain interactions J_a and J_b. These interactions couple the spins between the A-A or B-B type chains.

Finally, there are frustrating diagonal interactions between the A and B sublattices. The space group $P2_1/n$ differentiates two types of such diagonal couplings, which we denote as J^1_{AB} and J^2_{AB}. One may expect J^1_{AB} to be somewhat stronger within this pair, as the corresponding distance between the ions is about 1% shorter than for J^2_{AB}. We believe this inequality together with the special geometric pattern to be the key for understanding the peculiar spiral ground state. As the minimal toy model for interchain coupling, one can consider only J^1_{AB} and J_b, as shown in Fig. 9(b). Then the triangular layers are formed in the diagonal planes, with exchange J_b in the base of a triangle and J^1_{AB} along the sides [Fig. 9(c)]. Then the 2D propagation vector within this plane is given by $\cos(\mathbf{Q}' \cdot \mathbf{b}) = J^1_{AB}/2J_b$, being incommensurate only along the b direction. Note that this incommensurability stems exclusively from the competition of two weak exchange interactions and does not involve the intrachain exchange interaction J. This is the reason for the relatively large pitch angle of 108° between the A and B chain sublattices. At the same time, the strong intrachain interaction J promotes the antiparallel spin arrangement along the c axis, eventually leading to the 3D ordering wave vector $\mathbf{Q} = (0.5, Q^b_{inc}, 0.5)$, as observed experimentally. While this toy model captures the incommensurate ground state qualitatively, additional density functional theory (DFT) calculations would be desirable to establish the actual hierarchy of the relevant magnetic interactions and allow for a quantitative description.

In addition to revealing the frustrated nature of the interchain interactions, the observation of the incommensurate order also calls for revision of the antiferromagnetic resonance below T_N, reported by Okuda and Kadowaki [24]. The antiferromagnetic resonance in spiral structures is known to be rather different from simple collinear cases (see, e.g., [35]). The low magnitude of the ordered moment also stresses the importance of quantum fluctuations even far below T_N and hints to the possibility of observing characteristic 1D features at energies exceeding the interchain coupling [36].

IV. CONCLUSIONS

We presented systematic EPR and neutron-diffraction studies of the spin-1/2 Heisenberg AF chain compound $Cu(py)_2Cl_2$. Our EPR studies revealed a very small magnetic anisotropy ($\delta \sim 0.04$–0.06% of J). The angular dependence of the EPR linewidth strongly suggests an important role of the interchain geometrical frustration as a reason for the helical magnetic structure observed below T_N.

ACKNOWLEDGMENT

This work was partially supported by Deutsche Forschungsgemeinschaft and Swiss National Science Foundation (Division II). We acknowledge the support of the HLD at HZDR, member of the European Magnetic Field Laboratory (EMFL).

[1] V. Sachdev, *Quantum Phase Transitions* (Cambridge University Press, Cambridge, 1999).

[2] L. D. Faddeev and L. A. Takhtajan, Phys. Lett. A **85**, 375 (1981).

[3] D. C. Dender, P. R. Hammar, D. H. Reich, C. Broholm, and G. Aeppli, Phys. Rev. Lett. **79**, 1750 (1997).
[4] R. Feyerherm, S. Abens, D. Gunther, T. Ishida, M. Meissner, M. Meschke, T. Nogami, and M. Steiner, J. Phys. Condens. Matter **12**, 8495 (2000).
[5] M. Oshikawa and I. Affleck, Phys. Rev. Lett. **79**, 2883 (1997).
[6] I. Affleck and M. Oshikawa, Phys. Rev. B **60**, 1038 (1999).
[7] I. Affleck and M. Oshikawa, Phys. Rev. B **62**, 9200 (2000).
[8] F. H. L. Essler, Phys. Rev. B **59**, 14376 (1999).
[9] F. H. L. Essler and A. M. Tsvelik, Phys. Rev. B **57**, 10592 (1998).
[10] F. H. L. Essler, A. Furusaki, and T. Hikihara, Phys. Rev. B **68**, 064410 (2003).
[11] S. A. Zvyagin, A. K. Kolezhuk, J. Krzystek, and R. Feyerherm, Phys. Rev. Lett. **93**, 027201 (2004).
[12] H. Nojiri, Y. Ajiro, T. Asano, and J. P. Boucher, New J. Phys. **8**, 218 (2006).
[13] S. A. Zvyagin, E. Čižmár, M. Ozerov, J. Wosnitza, R. Feyerherm, S. R. Manmana, and F. Mila, Phys. Rev. B **83**, 060409(R) (2011).
[14] E. G. Cox, E. Sharratt, W. Wardlaw, and K. C. Webster, J. Chem. Soc., 129 (1936).
[15] M. Yokota and S. Koide, J. Phys. Soc. Jpn. **9**, 953 (1954).
[16] J. D. Dunitz, Acta Crystallogr. **10**, 307 (1957).
[17] K. Takeda, S. Matsukawa, and T. Haseda, J. Phys. Soc. Jpn. **30**, 1330 (1971).
[18] K. Takeda, Y. Yamamoto, and T. Haseda, Phys. Lett. A **45**, 419 (1973).
[19] T. Yamada, Y. Ajuro, S. Matsukawa, and T. Haseda, Phys. Lett. A **51**, 330 (1975).
[20] Y. Endoh, G. Shirane, R. J. Birgeneau, P. M. Richards, and S. L. Holt, Phys. Rev. Lett. **32**, 170 (1974).
[21] W. Duffy and J. E. Venneman, Phys. Rev. B **9**, 2220 (1974).
[22] B. Morosin, Acta Crystallogr. **31**, 632 (1975).
[23] I. U. Heilmann, G. Shirane, Y. Endoh, R. J. Birgeneau, and S. L. Holt, Phys. Rev. B **18**, 3530 (1978).
[24] K. Okuda and K. Kadowaki, J. Phys. Soc. Jpn. **46**, 45 (1979).
[25] A. M. C. Tinus, F. Boersma, and W. J. M. de Jonge, Phys. Lett. A **86**, 300 (1981).
[26] M. Thede, F. Xiao, Ch. Baines, C. Landee, E. Morenzoni, and A. Zheludev, Phys. Rev. B **86**, 180407(R) (2012).
[27] J. A. Chakhalian, R. F. Kiefl, R. Miller, J. Brewer, S. R. Dunsiger, G. Morris, W. A. MacFarlane, J. E. Sonier, S. Eggert, I. Affleck, A. Keren, and M. Verdaguer, Phys. Rev. Lett. **91**, 027202 (2003).
[28] M. Oshikawa and I. Affleck, Phys. Rev. Lett. **82**, 5136 (1999).
[29] M. Oshikawa and I. Affleck, Phys. Rev. B **65**, 134410 (2002).
[30] A. A. Zvyagin, Phys. Rev. B **63**, 172409 (2001).
[31] A. A. Zvyagin, Phys. Rev. B **79**, 064422 (2009).
[32] A. A. Validov, M. Ozerov, J. Wosnitza, S. A. Zvyagin, M. M. Turnbull, C. P. Landee, and G. B. Teitel'baum, J. Phys. Condens. Matter **26**, 026003 (2014).
[33] C. P. Slichter, *Principles of Magnetic Resonance* (Springer, Berlin, 1990).
[34] We found an R factor of 22% and $\chi^2 = 4.4$ for this solution.
[35] L. E. Svistov, L. A. Prozorova, M. Farutin, A. Gippius, S. Okhotnikov, A. Bush, E. Kamentsev, and A. Tishchenko, J. Expt. Theor. Phys. **108**, 1000 (2009).
[36] A. I. Smirnov, K. Yu. Povarov, S. V. Petrov, and A. Ya. Shapiro, Phys. Rev. B **85**, 184423 (2012).